Chapter 5. Dynamics of material removal

5.1 Femtosecond laser pump-probe measurements: Ions

More insight into the mechanisms involved in the material removal from laser irradiated surfaces can be gleaned from time-resolved measurements using femtosecond laser pump-probe experiments. Such studies allow one to derive detailed information on the times relevant for energy coupling into the lattice and the redistribution channels. For the first set of these experiments we have used two laser pulses of 80 fs duration and equal pulse energies, each individual pulse energy lying below the ablation threshold but their sum exceeding the threshold of 3.5 J/cm^2 for sapphire. The two pulses are separated by a variable time delay (see Chapter 2 for experimental details). The key question here is how long the material remembers that it has been pre-treated by the pump pulse. We have to remember at this point that due to a defect accumulation process, the ablation threshold decreases with N, the number of consecutive pulses per site (as demonstrated in Chapter 3). For the present studies the pump fluence has been chosen in such a way (below the ablation threshold for two successive pulses on the same irradiated site) that no observable permanent modifications occur after the pump irradiation, the surface viewed by the second pulse remaining unchanged. Sample cooling, and heat dissipation cause the pump-probe signal to drop to zero for long delay times, so that any effect of the pump pulse remains reversible. If the fluence is increased between the threshold for the second successive pulse and the threshold for the first pulse, it is likely that permanent modification, radiation induced defects, will make the signal reach a non-zero steady-state value. The quantity of interest, the ion yield, was measured at different pump-probe delay times as an indication of the redistribution channels for energy accumulation in the sample.

The ion yield was recorded with the TOF-mass spectrometer (see Chapter 2), the sample surface being parallel to the extraction grids. A new spot on the surface was chosen for each data point as the delay was varied. The results are shown in Fig. 5.1-1 (a). The ion signal was measured at a fixed extraction time in the mass spectrometer so that a well-defined velocity of ~20300 m/s was selected for the detected ions, with the TOF operating as a velocity filter.

It is useful to assume for a qualitative description that the first pulse induces a certain quantity of “excitation”, i. e. density of free electrons, hot electron distribution, electrostatic

energy (positive charge accumulation on the surface following the electron photoemission) or thermal energy transferred to the lattice. Each of these channels has a characteristic relaxation time and the magnitude of this laser induced “excitation“ changes with time after the pulse ends. This “excitation” initially induced with only one sub-threshold beam is not enough to exceed the threshold for the ablation process so that no ion yield is detected solely with the pump pulse (or the probe pulse) alone. The “excitation” produced by the second (probe) pulse adds to the remaining excitation from the first pulse, and may thus exceed the ablation threshold. In the latter case an ion signal is detected. This ion signal is recorded as a function of the delay time Δt between pump and probe pulse and contains information on the laser energy deposition dynamics.

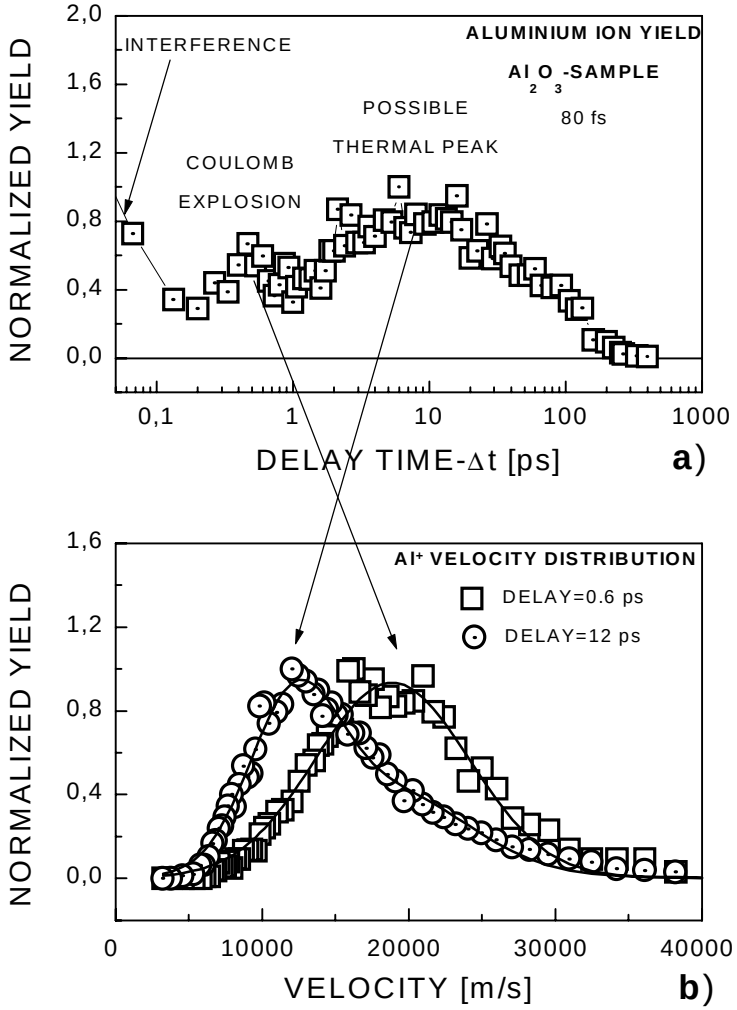

Fig. 5.1-1 a) Pump-probe measurement for Al_2O_3 (fast Al^+ ion yield, v=20300 m/s, see text for details) with 80 fs pulses of equal pulse energy (below the threshold for N=2 (<3 J/cm^2)).
b) Velocity distributions at different delay times, showing that ions produced for low pulse delay times (< 1 ps) have velocities corresponding to the Coulomb explosion mechanism whereas ions produced with larger pulse delay times have lower velocities indicating a thermal mechanism.

It is essential to note that we are probing the “excitation” accumulation at the level of the lattice, i.e. different forms of energy (electrostatic, thermal) deposited into the lattice with consequent surface damage. The ion signal is regarded as a measure of the balance between induced electrostatic and thermal energy. The pump-probe signal is not directly related to the temporal onset of ion emission (the moment of ion ejection) but gives the characteristic times for different energy deposition channels into the lattice, energy that is the cause for ion removal through different mechanisms described in the precedent chapters.

The temporal behavior of the ion yield depicted in Fig. 5.1-1 exhibits a multiple peak structure.

- The initial maximization at zero delay
- The first peak at about 600 fs
- The second peak at around 10 ps.

1) A strong ion signal is observed for zero delay, i.e. when the two laser pulses overlap on the surface at the same time, an effect that is due to the coherent superposition of the laser beams for delay times up to 130 fs (the autocorrelation time) and optical interference. The corresponding minimum at 0.1 ps has the same source. These features are without relevance for the understanding of the ablation process.

2) After an initial decrease due to interference effects, the signal rises to a first peak and then decreases again, reaching a minimum at around 1 ps. We take this to reflect the initial electrostatic energy accumulation at the surface (arguments are given below).

The first fast peak, which is attributed to ion emission driven by electrostatic repulsion, gives direct evidence for Coulomb explosion. It was demonstrated in Chapter 4 that this repulsion is generated by the strong photoelectron emission and, hence, remaining positive charges on the surface.

The second peak originates from thermal effects (on a time comparable to the electron-lattice relaxation time as will be seen below).

For delay times less than 1 ps the energy induced by the first pulse is accumulated as both hot free electron distribution and electrostatic energy on the surface due to a breakdown of quasi-neutrality in the first surface layers. The pump-induced charge is at a sub-critical magnitude to generate the surface break-up. The second laser pulse induces additional surface charge and, when the total charge density is sufficient to overcome the binding energy of the lattice and to generate the surface break-up by Coulomb explosion, ions are detected. The surface charge build-up is reflected by the maximum around 600 fs which can be explained in terms of efficient photoemission from the hot but thermalized electrons (electron-electron

collisions will induce a rapid redistribution of energy into the electronic system in order to establish a hot Fermi distribution with a high temperature that decreases afterwards due to electron-phonon coupling). This may induce an enhanced coupling of the second pulse after some relaxation of the initially excited electrons (produced by the first pulse), related to carrier-carrier equilibration, and, therefore extra-charging.

The combined charge density (the common contribution of the two pulses) decreases below the surface break-up threshold after a delay of about 1 ps due to the reduction in the charge density that has been induced by the first laser pulse. We believe that this gives evidence for a timescale through which the charge distribution at the surface, initiated by the first laser pulse can remain stable above the critical value. The induced positive charge in the electron depleted region decays due to effects such as e.g. individual (i.e. not bulk ablation because the pump pulse itself is not able to induce macroscopic ablation) ion ejection from the surface, hole diffusion from the irradiated area and, more important, electron supply from the bulk. We have seen in Chapter 4 that the depleted region has a depth of about 2-3 nm (10 % from the one shot induced modification in the gentle phase), in good agreement with the electron escape depth [Hüf95, Hui99]. In delayed neutralization which takes place in the electron depleted region (positively charged) electron diffusion and their drift in the induced electric field plays a very important role. The neutralization process is depicted in Fig. 5.1-2.

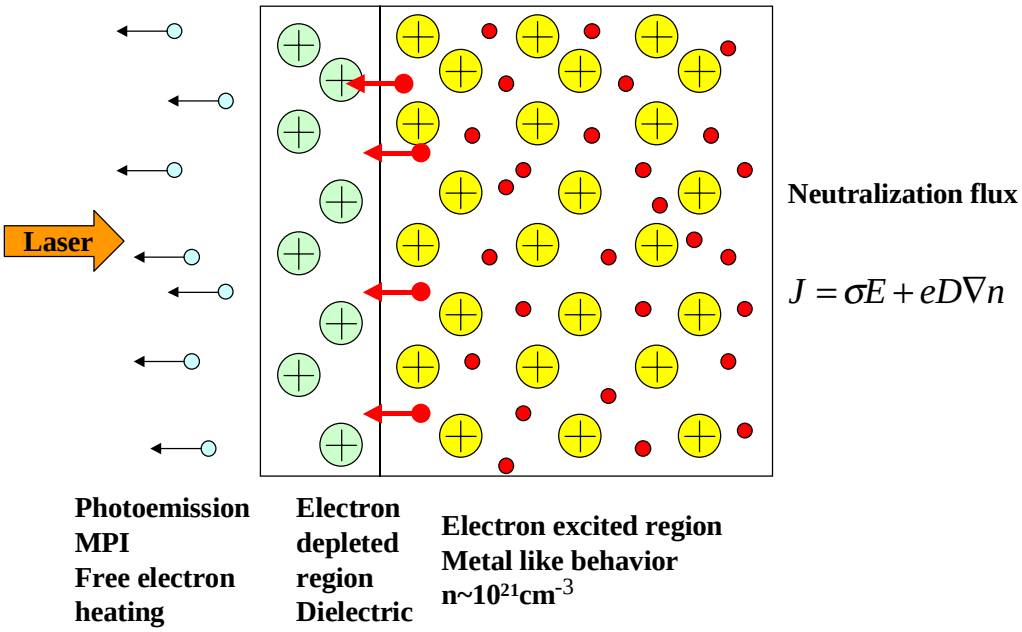

Fig. 5.1-2 Sketch of the neutralization process in the electron depleted region. n is the electron density, J is the charge flux, σ is the electrical conductivity, e is the electron charge and D is the diffusivity coefficient. Note the charge flow from the excited region to the depleted region and subsequent neutralization [See91].

3) The second rise of the signal (between 1 and 10 ps) is attributed to lattice heating due to electron-phonon coupling.

In addition to the mechanisms involved in the charge neutralization, another process is responsible for the lowering of the efficiency of the probe to induce extra-charging. The residual excited electrons in the surface region will decay via electron-phonon coupling on the ps timescale. This leads to heating of the lattice, adds to the enhancement of the second peak (better coupling of the probe pulse on a heated surface), and also reduces the efficiency of the surface ionization induced by the second pulse.

In order to obtain more information about the nature of the observed signal we have measured the velocity distribution for the ions corresponding to the first, fast peak and to the second, slower peak of possible thermal nature, respectively. The velocity distributions for the Al^+ ions are depicted in Fig. 5.1-1 (b). The most probable velocity characterizing the particles from the first fast peak is higher than the velocity of the maximum corresponding to the second peak.

The velocity distributions of the ions produced for pump-probe delays up to ca. 1 ps strongly resemble those of the fast Coulomb explosion as illustrated in Fig. 5.1-1 (b) for a time delay of 600 fs, thus supporting the hypothesis of an electrostatic repulsion driving the first peak. The dynamics involved in the fast ion formation relies, as was discussed, on the availability of appreciable electron density in the conduction band and sufficient charging.

After the charge decay, beyond 1 ps, an increase in the ion production can again be noticed, peaking at about 10 ps. This second feature originates most probably from thermal deposition of energy in the sample. The ions produced on this time scale have velocity distributions similar to the low velocity, thermal distributions with almost equal energies for the two mass species rather than equal momenta as discussed in Chapter 4. This time scale is characteristic for the time scale for electron-phonon coupling and surface heating. Electron-phonon coupling removes energy from the electronic degrees of freedom so that the second laser pulse can no longer sufficiently ionize the surface region to produce significant Coulomb explosion. Instead, much of the total input energy is converted to lattice motion leading to the thermal removal of neutrals and ions on a time scale of tens of ps. It is reasonable to believe that, on this time scale, the energy is transferred to the lattice via electron-phonon collisions in a thermal fashion without preferential decay channels, leading to a temperature increase in the affected region and phase-transition. This is equivalent to extreme heating of the sample on this time scale followed by thermal ejection of ions and then, subsequent cooling. This also explains the observed low velocity component in the ablation process by a single 2.8 ps laser

pulse (Fig. 4.1-17). There is sufficient time during the picosecond laser pulse for electronic energy to be efficiently coupled to the thermal motion of the lattice which subsequently leads to low velocity ion removal. (The velocity of the ions even in the ”low” velocity signal is still rather large, implying that hydrodynamical effects in the plume of ablated material are significant and lead to a high stream velocity).

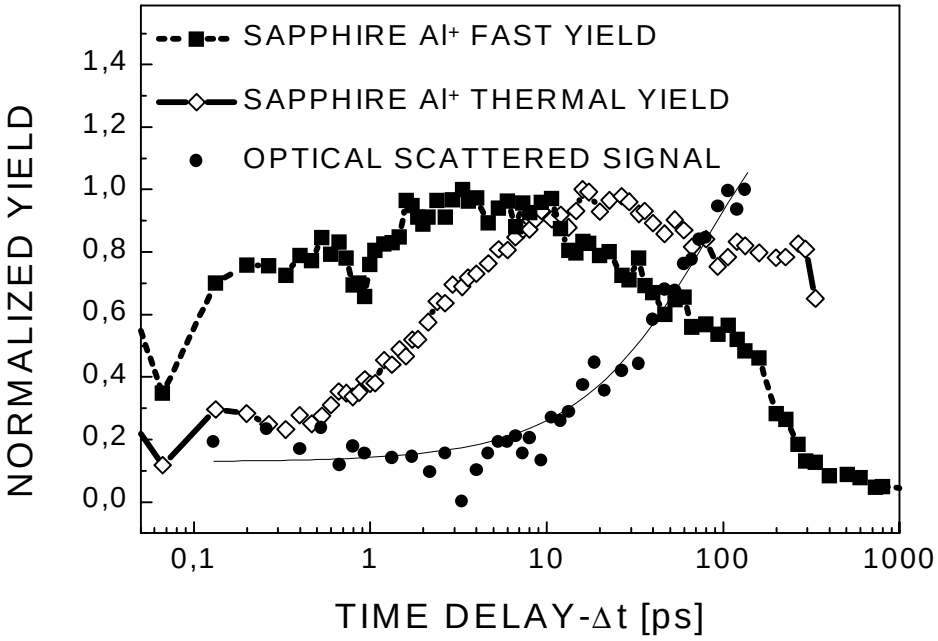

Fig. 5.1-3 Dependence of Al^+ ion intensity on the delay between two laser pulses of equal fluences at 100 fs irradiation. The individual pulse fluences are below the ablation threshold but the sum lies above (F_{th}=3.5 J/cm^2). Black squares: fast ions with a velocity of 20300 m/s. Open diamonds: slow ions with a velocity of 12000 m/s. The minimum at 70 fs is an artifact due to interference between the two overlapping laser pulses. Black circles: data on the time dependence of scattered light from material leaving the surface (mainly neutral particles), from [RAV1998], shown for comparison.

So, in contrast to the short time behavior, at long delay times (10 ps) the second laser pulse couples better with the heat bath of the lattice after the electrons have released their energy to the lattice.

The observed decay of the pump-probe ion signal for delays greater than 10 ps may have two origins. Petite and co-workers have shown that the electrons remain trapped either in or close below the conduction band on a time scale of about 100 ps [PDG96]. From these excited states efficient low-order excitation can occur which can be more efficient than the high-order excitation of electrons in the valence band. When these states decay (after 100 ps), the energy of the second laser pulse can no longer be efficiently coupled into the system and can no longer lead to significant ion removal.

Secondly, and perhaps more importantly in the range 10-100 ps, thermal diffusion will start to become significant thus reducing the total thermal excitation in the area irradiated by the first laser pulse. The characteristic thermal diffusion length $L_{th} = \sqrt{2D_{th}\tau}$ is on the order of tens up to hundreds of nanometers (thermal diffusion has a characteristic time on the tens of ps time scale) and the electron diffusion length has similar dimensions. Here D_{th} is the thermal diffusivity and τ is the characteristic time involved in the thermal process, (for longer pulses, e.g. ns pulses, and short absorption length $L_{abs}=1/\alpha_{abs}<L_{th}$, τ becomes the pulse duration that controls the thermal diffusion process).

In a second experiment the ion signal was recorded as a function of the delay between the two pulses for two different ion velocities (in this case the pulse duration was 100 fs). The results for the Al^+ ions are shown on Fig. 5.1-3. The ion velocities were 20300 m/s (black squares), corresponding to the fast, Coulomb explosion ion distribution (Fig. 5.1-1 (b)) and 12000 m/s, corresponding to the most probable velocity of the slow, thermal distribution (open diamonds). For comparison we also show earlier results on the intensity of the scattered light signal as a function of delay time (black circles). These data were taken with a strong first pulse (10 J/cm^2) to initiate ablation and the timescale for bulk material removal was probed by the light scattered from the second, weaker pulse as a function of delay time [RAV98]. The fast ions (solid squares) in the present experiments follow a similar behavior as in the initial, 80 fs, experiment. Again, as in Fig. 5.1-1 we observe the first peak generated by surface charging and Coulomb explosion break-up. The signal of fast ions that also rises again and is observed up to 200 ps delay is thought to be due to the high temperature tail of the thermal ion distribution (Fig. 5.1-3) and to have thus a different origin from the signal that starts to decay at about 1 ps. The slower, thermal ions (open diamonds) beginning to be observed after a delay of about 1 ps show an increase to a maximum at 10 ps due to the transfer of electronic energy to the lattice and subsequent heating. This signal is the signature of a high surface temperature. As we have argued before, for delay times beyond about 1 ps the second pulse thus can not induce sufficient charge density to lead to macroscopic Coulomb explosion, rather the additional energy input will be used predominantly for heating of the lattice. The time scale for the additional heating due to the second laser pulse will also be 1-10 ps. In contrast to the very fast removal of the surface ions due to Coulomb explosion, the thermal removal of the bulk material will thus take longer. This is nicely supported by the time behavior of the scattered light that indicates when the bulk of the material leaves the surface [RAV98]. Our pump-probe ion signal is indicating that the maximum lattice

temperature is reached after 10 ps. This is in good agreement with the scattered light signal that indicates the onset of the bulk thermal material removal after about 10 ps.

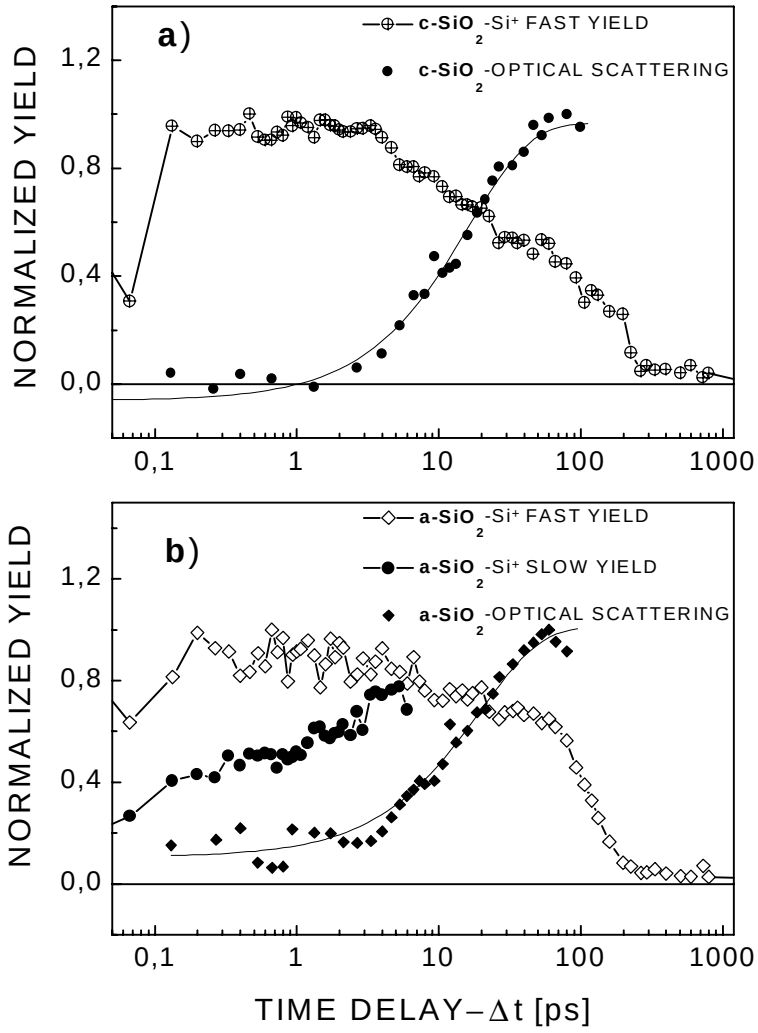

Fig. 5.1-4 Si^+ ions TOF pump-probe experiments of crystalline quartz (a) and fused silica (b). Note the early contribution in the signal for fast particles and the thermal feature indicated by the slow particles. The scattered light signal is also represented.

Similar behavior has been observed for other dielectric materials, fused silica and crystalline quartz as is shown in Fig. 5.1-4.

Again, the fast, non-thermal peak of ions with velocities of ~20300 m/s originating from Coulomb explosion is visible for sub-ps delay times. As in the case of the Al_2O_3, the low velocity signal (~12000 m/s) originating from the low energy tail of the thermal distribution is a signature of the surface temperature. It should be noted that the heating process is faster than for Al_2O_3 consistent with the fast electron trapping process in self-trapped exciton states (STE's) [PDG96] on a time scale of 150 fs. The strong coupling between STE's and the lattice leads to a more efficient energy transfer to the thermal channel. Fused silica and quartz

exhibit a much higher electron-phonon coupling strength as compared to sapphire. The correlation with the scattered optical signal from the irradiated spot that is regarded as the onset of the ablation process supports nicely this picture. This type of behavior is characteristic for dielectrics as a consequence of the fact that the induced positive charge is not neutralized fast enough to prevent ion repulsion. In contrast, excited semiconductors like laser irradiated silicon (Si) show different dynamics. No fast (Coulomb explosion) peak is observed for excited semiconductors, impeded by the extremely swift charge flow from the excited region into the electron-depleted region. The situation remains the same for other types of higher electrical conductivity materials.

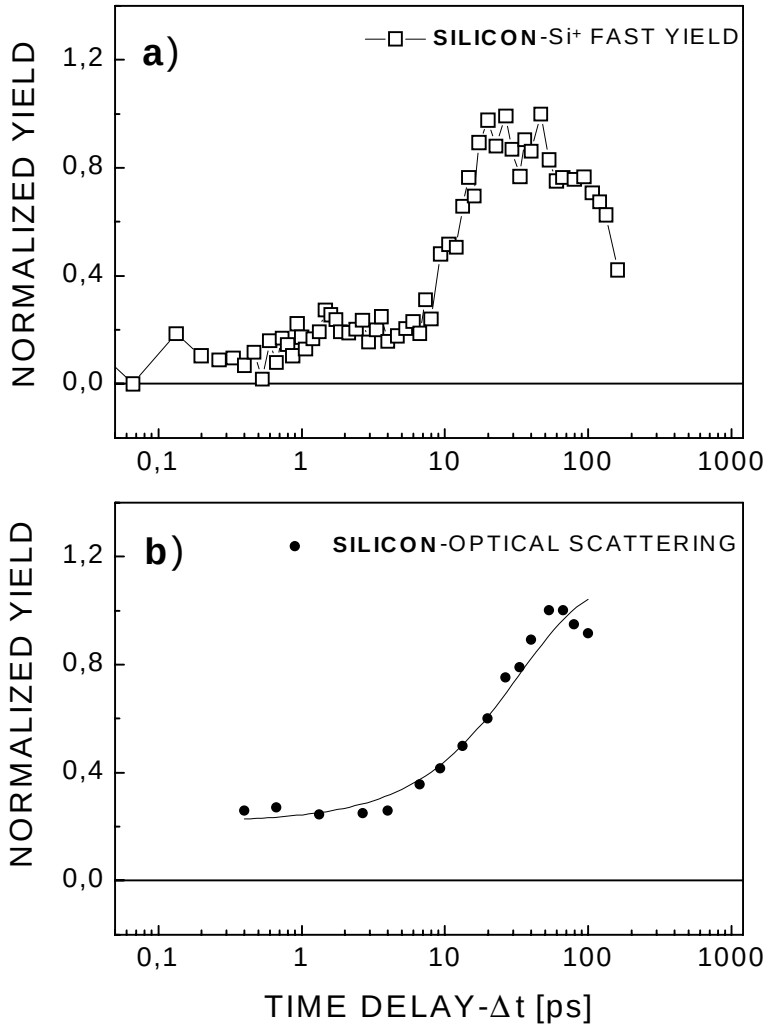

Fig. 5.1-5 Si^+ ions TOF pump-probe experiment on silicon sample (a). No fast peak is present. For comparison purposes the scattered signal is also indicated (b).

Rather, an increase in the ion yield after a few (5-10) ps is seen i.e. on the time scale of heat conduction in Si (Fig. 5.1-5, and Fig. 5.1-6). This gives evidence of a genuine thermal

process [SYC83, DFS85, SBC98, CSB99, SCS99, and the references therein]. (For silicon an electron-electron thermalization time of less than 120 fs has been reported [GoP93], an extremely fast initial electron cooling rate, followed by an electron-phonon thermalization time of approx. 1 ps together with a strong energy dependence of the electron scattering rates. However, the sample may experience significant hot electron diffusion during this time, this being the relevant parameter of energy deposition [GHM98]).

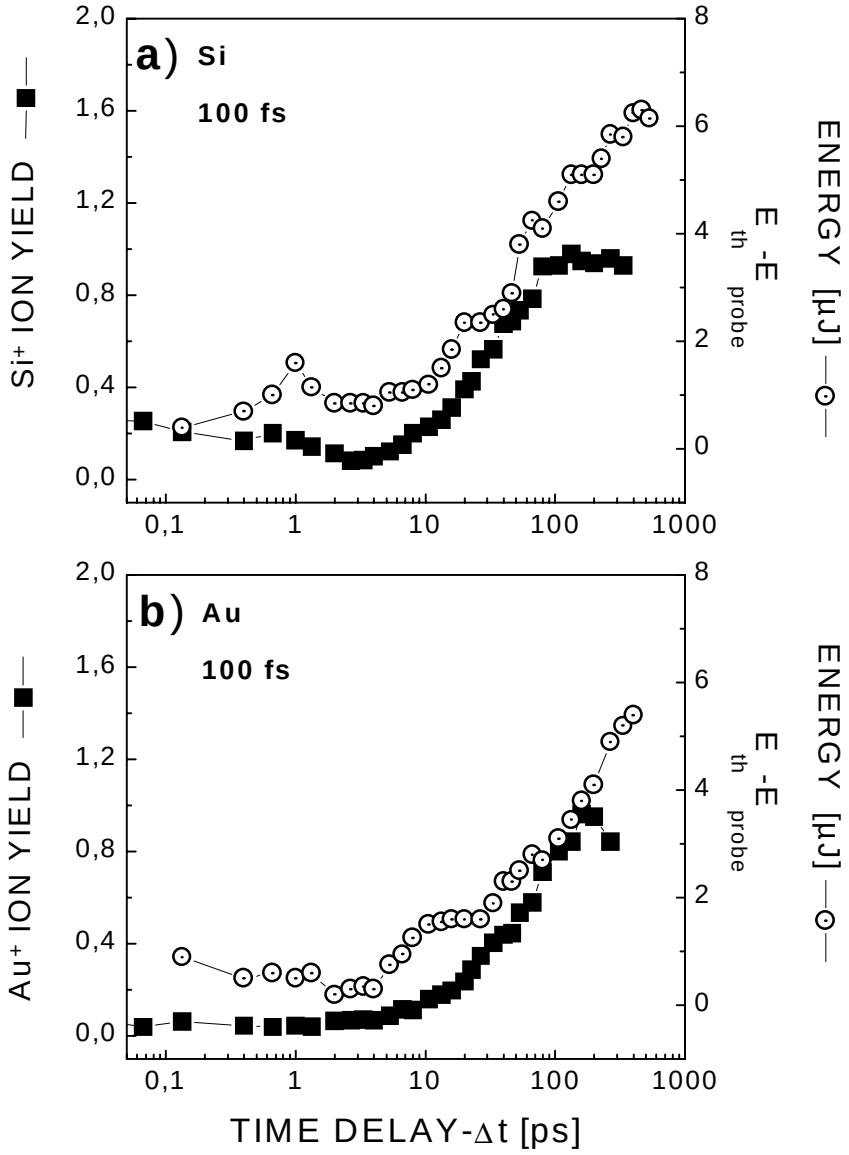

Fig. 5.1-6 Si^+ (a) and Au^+ (b) ions TOF yield and ablation energy threshold (signaled by the ion burst) pump-probe experiment on silicon and gold samples (see text for details).

Optical microscope studies demonstrated that after this time (5-10 ps corresponding to the ion yield onset), structural modification accompanied by a solid-to-liquid transition

(witnessed by the solidified melt and ripple formation) of the target occur, increasing the coupling efficiency between the laser and the Si sample. In an attempt to clarify this observation we have to add that Si experiences two very distinctive thresholds, one which can be defined as the melting threshold with almost no ions emitted from the surface at about 0.2 J/cm^2 and the other one associated with ablation and ion emission at about 1 J/cm^2. That means the silicon (and also metals) needs much more energy to vaporize than to melt. In our experiments the pump fluence was slightly below the ion emission threshold but both individual pulses were above the melting threshold. For comparison, we have also performed light scattering experiments with the pump beam fluence above the ion emission threshold. The results are reported in Fig. 5.1-5. It also shows an onset of particle removal after a few ps (Fig. 5.1-5). Comparable behavior has been noted for metals. This is exemplified in Fig. 5.1-6 for a sample of 1 µm gold thin film on a fused silica substrate. Gold is a ductile metal and, consequently, the first step in optical damage is surface melting. The energy penetration depth is about 500 nm and it is due to hot electron diffusion controlling the heat transport in the target [GHM98]. Unlike the dielectrics, for semiconductors and metals Coulomb explosion will have a very low probability due to neutralization of the accumulated charge by electron transport to the interaction region which is facilitated by the high carrier mobility [HMW97, WRL94, MDF2000].

The above-presented studies have underlined the significance of both nonthermal and thermal processes in ion removal when using ultrashort laser pulses for the ablation of dielectrics. An electrostatic repulsion mechanism is responsible for fast ions during the first ps after the excitation. Then the balance shifts towards thermal processes on a time scale of tens of ps, given by the free electron lifetime, electron-phonon coupling and heat conduction. In the case of silicon, the energy is deposited into the target in a time determined by heat conduction so that a thermal mechanism for expulsion (govern by phase-transformation temperatures) prevails. The same conclusions can be drawn from another type of the experiment, which measures the probe energy E_{probe} necessary to reach the threshold (at an electron density close to the critical density of ~10^{21}cm^{-3}). In this experiment the pump energy was kept constant at a sub-threshold value, while the probe pulse energy was adjusted for each delay times in order to reach ion emission threshold. This quantity "$E_{threshold}$-E_{probe}" can be regarded as a measure of the induced excitation (i.e. a measure of the excitation present in the sample at the moment of the probe arrival), and its dependence on the delay time is similar to the trend in the TOF pump-probe measurements (Fig. 5.1-6)

5.2 Femtosecond pump-probe measurements: Emitted electrons

In an effort to elucidate the nature of the induced excitation for dielectric materials we have also measured the electron yield emitted from a sapphire irradiated surface. It was shown in Chapter 4 that for 200 fs IR irradiation, the electron time-of-flight distributions contains a contribution from fast, prompt electrons, with energies in the range of eV followed by the slow electrons (electrons that travel along the plume), having energies in the meV range. The situation remains similar for 100 fs irradiation (Fig. 5.2-1). Each of the two distributions are normalized to the maximum value, i.e. the magnitudes are not correlated. It has been show by Daguzan et al. [DGK94] that for long wavelengths one of the main processes for fast electron photoemission is free carrier absorption, shifting to direct multiphoton emission for smaller wavelengths.

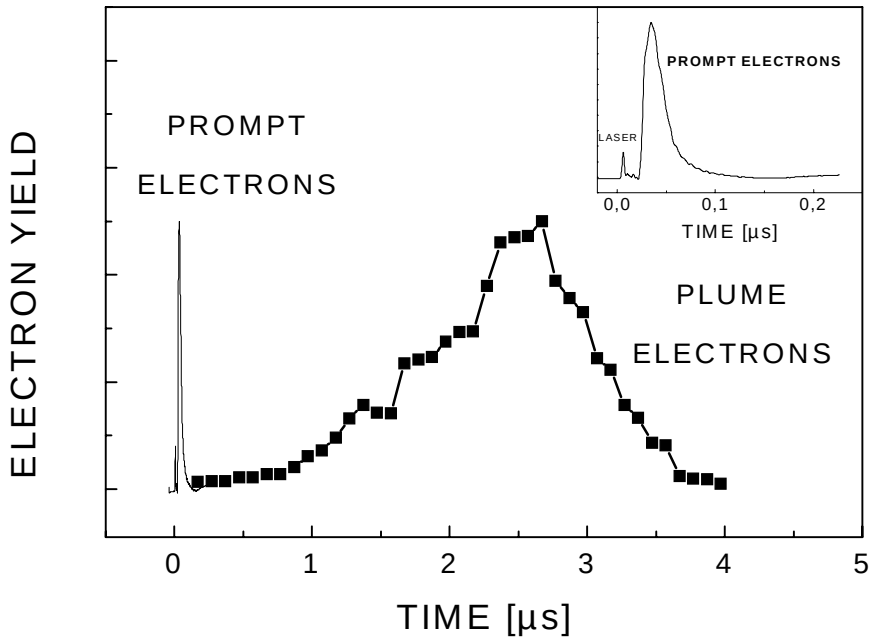

Fig. 5.2-1 TOF electron distribution for 100 fs laser irradiated sapphire at 3.9 J/cm^2. One can note the presence of the prompt, fast electrons, as well as the delayed slow electrons accompanying the plume.

We have performed the same type of pump-probe experiment monitoring the prompt electron signal as a function of the probe delay. The results are presented in Fig. 5.2-2. Again, both pump and probe pulses were at subthreshold fluences and have almost equal intensities.

In this case no signal is detected with only one beam. The measured yield is the result of the cooperative interaction between the induced effects of each of the two pulses. The prompt electrons temporal behavior follows closely the same dependence as the Coulomb explosion ion peak (first peak) reported above in the ion dynamics experiment. This constitutes another strong support for the assumption of an initial emission due to positive electrostatic repulsion of ions.

It has thus been argued that the prompt electron emission constitutes the cause of the observed repulsive ion ejection. Prompt electron emission leads to the neutrality break-up in the first surface layers and initiates the ion Coulomb explosion. In the pump-probe electron experiments care has been taken to minimize the electron contribution from the surface H sites (water contamination of the surface). To do this, a succession of pump-probe sequences was employed at a repetition rate of 5 Hz. The first pump-probe flash effect was to clean the surface prior to collecting the electron signal data, while the electron yield has been recorded for the second irradiation sequence. Also attention has been paid to minimize the contribution of plume electrons in the prompt peak since we were working with a bias voltage for electron extraction of 200V, applied on the sample. The voltage used was, on the one hand, strong enough to collect the prompt electrons but, on the other hand, it was too small to initiate any plume depletion of electrons.

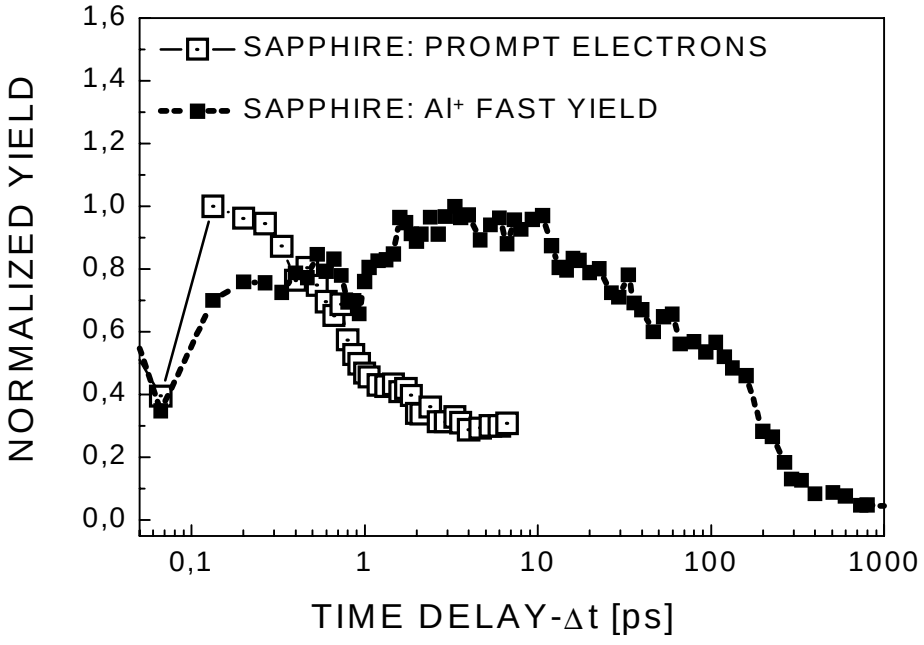

Fig. 5.2-2 Temporal evolution of the prompt electron signal as a function of the pump-probe delay time for laser irradiated sapphire. The correlation with the temporal behavior of the fast, Coulomb explosion ions is observable.

5.3 Summary

This chapter has presented time-resolved ion and electron investigations based on two identical pulses correlation technique. The photoemission induced uncompensated positive charge on dielectric surfaces can survive at surface break-up values up to 1 ps, leading to an electrostatic ion emission by Coulomb explosion, as evidenced by the fast ions and prompt electrons measurements. Unlike dielectrics, for metals and semiconductors, fast charge neutralization will inhibit any Coulomb explosion manifestation. Surface heating (revealed by the slow ion yield) is found to be on the ps time scale controlled by the material dependent electron-phonon coupling. The high temperatures of the surface determine the phase transformation and lead to thermal emission of particles with lower velocities as compared to the electrostatic repulsion.